THE JOURNAL OF BIOLOGICAL CHEMISTRY VOL. 288, NO. 21, pp. 14824–14838, May 24, 2013

Transforming Growth Factor-β1 (TGF-β1)-stimulated Fibroblast to Myofibroblast Differentiation Is Mediated by Hyaluronan (HA)-facilitated Epidermal Growth Factor Receptor (EGFR) and CD44 Co-localization in Lipid Rafts*

Received for publication, January 8, 2013, and in revised form, March 27, 2013 Published, JBC Papers in Press, April 15, 2013, DOI 10.1074/jbc.M113.451336

Adam C. Midgley[‡], Mathew Rogers[‡], Maurice B. Hallett[§], Aled Clayton[¶], Timothy Bowen[‡], Aled O. Phillips[‡1], and Robert Steadman[‡1,2]

From the [‡]Institute of Nephrology and [§]Neutrophil Signalling Group, Institute of Molecular and Experimental Medicine, School of Medicine and Cardiff Institute of Tissue Engineering and Repair, University of Cardiff, Heath Park, Cardiff CF14 4XN, United Kingdom and the [¶]Institute of Cancer and Genetics, School of Medicine, Cardiff University, Velindre Cancer Centre, Whitchurch, Cardiff CF14 2TL, United Kingdom

Background: Wound healing and scarring are driven by transforming growth factor-β1 (TGF-β1)-dependent fibroblast to myofibroblast differentiation.
Results: Cell surface CD44 and epidermal growth factor receptor (EGFR) co-localize in lipid rafts to signal through mitogen-activated protein kinase 1/2 (ERK1/2) and Ca^{2+}/calmodulin kinase II (CaMKII).
Conclusion: CD44 moves into lipid rafts in a TGF-β1- and hyaluronan-dependent manner, co-localizes with EGFR, and triggers differentiation.
Significance: This pathway presents novel targets for the therapy of wound-healing and fibrosis.

Fibroblast to myofibroblast differentiation drives effective wound healing and is largely regulated by the cytokine transforming growth factor-β1 (TGF-β1). Myofibroblasts express α-smooth muscle actin and are present in granulation tissue, where they are responsible for wound contraction. Our previous studies show that fibroblast differentiation in response to TGF-β1 is dependent on and mediated by the linear polysaccharide hyaluronan (HA). Both the HA receptor, CD44, and the epidermal growth factor receptor (EGFR) are involved in this differentiation response. The aim of this study was to understand the mechanisms linking HA-, CD44-, and EGFR-regulated TGF-β1-dependent differentiation. CD44 and EGFR co-localization within membrane-bound lipid rafts was necessary for differentiation, and this triggered downstream mitogen-activated protein kinase (MAPK/ERK) and Ca^{2+}/calmodulin kinase II (CaMKII) activation. We also found that ERK phosphorylation was upstream of CaMKII phosphorylation, that ERK activation was necessary for CaMKII signaling, and that both kinases were essential for differentiation. In addition, HA synthase-2 (HAS2) siRNA attenuated both ERK and CaMKII signaling and sequestration of CD44 into lipid rafts, preventing differentiation. In summary, the data suggest that HAS2-dependent production of HA facilitates TGF-β1-dependent fibroblast differentiation through promoting CD44 interaction with EGFR held within membrane-bound lipid rafts. This induces MAPK/ERK, followed by CaMKII activation, leading to differentiation. This pathway is synergistic with the classical TGF-β1-dependent SMAD-signaling pathway and may provide a novel opportunity for intervention in wound healing.

Fibroblasts are considered to be the primary source of the reparative matrix in all tissues. In response to injury, they proliferate, migrate to the site of injury, and differentiate into their activated form, myofibroblasts (1–3). Following differentiation, myofibroblasts acquire an increased contractile ability and are characterized by the expression of an α-smooth muscle actin (α-SMA)[3] positive phenotype (2). In wound healing, these myofibroblasts mediate wound contraction and the formation of a collagen-rich extracellular matrix (4). Increased activation and proliferation of resident fibroblasts at the wound edge is therefore an important early step that is central to the wound healing process.

The cytokine, transforming growth factor-β1 (TGF-β1) is a mediator of tissue repair and wound healing (5–8) and has also been widely implicated in progressive tissue fibrosis (9–11). In addition to its effect on extracellular matrix turnover, TGF-β1 is known to have direct effects on cell phenotype, including the induction of a contractile phenotype and the up-regulation of α-SMA both *in vitro* and *in vivo* (12, 13). TGF-β1, therefore, drives fibroblast-myofibroblast differentiation, and it has been previously demonstrated that the matrix polysaccharide hyalu-

* This work was supported in part by a studentship from Research into Aging/Age UK (Grant 358) (to A. M. and R. S.). This work was also supported by the Kidney Wales Foundation.
[1] Both authors contributed equally to this work.
[2] To whom correspondence should be addressed. Tel.: 2920-748390; Fax: 2920-748470; E-mail: steadmanr@cf.ac.uk.

[3] The abbreviations used are: α-SMA, α-smooth muscle action; EGFR, epidermal growth factor receptor; CaMKII, calcium-calmodulin kinase II; HA, hyaluronan; HAS2, hyaluronic acid synthase 2; TGF-βRI, transforming growth factor β receptor I; FRAP, fluorescent recovery after photobleaching; QPCR, quantitative PCR; TRITC, tetramethylrhodamine isothiocyanate; ICQ, intensity correlation quotient; Cav-1, caveolin-1; CTX-B, cholera toxin subunit B; CTX-HRP, cholera toxin subunit B-HRP conjugate; EEA-1, early endosome antigen 1; GM1, monosialotetrahexosylganglioside; PE-R, phycoerythrin red.

ronan (HA) plays a pivotal role in regulating TGF-β1 signaling (14) and TGF-β1-driven responses in fibroblasts (15).

HA is a linear glycosaminoglycan of the extracellular matrix involved in a range of cellular functions, including cell-cell adhesion, migration, proliferation, and differentiation, and it therefore plays an important role in wound healing and tissue repair (16–21). The biosynthesis of HA is regulated by three mammalian HA synthase isoenzymes, of which hyaluronan synthase 2 (HAS2) demonstrates the greatest expression in fibroblasts (22–25). We have previously shown that as a consequence of myofibroblastic differentiation, a pericellular coat of HA accumulated around differentiated cells (26). This HA pericellular coat was organized and regulated by the hyaladherin tumor necrosis factor-stimulated gene-6, and this was essential for the differentiation process together with the HA cell surface receptor (CD44) (27). In addition, the response to TGF-β1 was controlled by altering the levels of HA generated by the fibroblasts through overexpression of HAS2 or by blocking HA synthesis. However, the mechanism through which HA regulated TGF-β1-dependent differentiation, and thereby potentially influenced the wound healing response, is not yet fully understood.

Several studies have indicated that epidermal growth factor (EGF) enhanced the profibrotic effects of TGF-β1, (28–31) and that the transmembrane epidermal growth factor receptor (EGFR) is a key regulator of the response. We have shown that EGFR is an essential receptor in the differentiation and proliferation of fibroblasts, and its interactions with HA and CD44 are required for both cellular responses (32, 33). As fibroblasts age, they display a resistance to phenotypic activation (15, 22, 23, 34, 35), and we have shown that this is associated with loss of EGFR expression. This resistance was overcome by overexpression of EGFR with HAS2 (32), confirming that EGFR and HA are necessary components of the differentiation pathway in fibroblasts. We propose a model that involves two distinct but cooperating pathways: 1) TGF-β1/SMAD2-dependent signaling and 2) HA/CD44/EGFR-dependent signaling. In this study, we investigated the mechanisms underlying the HA-dependent regulation of fibroblast differentiation through CD44-EGFR and have further investigated the regulation of intracellular signaling pathways. We identified a population of CD44 in the cell membrane that relocated to EGFR held in lipid rafts. The CD44/EGFR co-localization induced p42/44 MAPK (ERK1/2) phosphorylation followed by calcium-calmodulin kinase II (CaMKII) phosphorylation. The mechanisms described here help to further explain fibroblast to myofibroblast differentiation.

EXPERIMENTAL PROCEDURES

Materials—All reagents were from Sigma-Aldrich unless otherwise stated. The primary antibodies and dilutions used for Western blot analysis were monoclonal mouse anti-EGFR (1:1000) and monoclonal rat anti-CD44 (1:5000) from Calbiochem; polyclonal rabbit anti-phosphorylated EGFR (dilution 1:5000), polyclonal rabbit anti-ERK1/2 (1:10000), monoclonal mouse anti-phosphorylated ERK1/ERK2 (1:10,000), polyclonal rabbit anti-CaMKII (1:5000), monoclonal rabbit anti-phosphorylated CaMKII (1:5000), monoclonal rabbit anti-Smad2 (1:5000), and polyclonal rabbit anti-phosphorylated Smad2 (1:5000) from Cell Signaling Technology, Inc. (Beverly, MA); and monoclonal mouse anti-TGF-βRI (1:1000) from Santa Cruz Biotechnology, Inc. (Santa Cruz, CA). Reverse transcription, small interfering RNA (siRNA) transfection reagents, and quantitative PCR (QPCR) primers and reagents were purchased from Invitrogen and Applied Biosystems (Cheshire, UK). Other reagents used were recombinant TGF-β1 from R&D Systems (Abingdon, UK), nystatin, EGFR inhibitor AG1478, ERK (MEK) inhibitor PD98059, and CaMKII inhibitor KN-93 from Calbiochem. Final working inhibitor DMSO concentrations were 0.06% (v/v); therefore, DMSO was added to cultures at 0.06% (v/v) as a solvent control.

Cell Culture—Primary human lung fibroblasts (AG02262; NIA, National Institutes of Health, Aging Cell Respiratory Corriel Institute) were cultured in Dulbecco's modified Eagle's medium (DMEM) and F-12 medium containing 2 mM L-glutamine, 100 units/ml penicillin, and 100 μg/ml streptomycin supplemented with 10% fetal calf serum (FCS) (Biological Industries Ltd., Cumbernauld, UK). The cells were maintained at 37 °C in a humidified incubator in an atmosphere of 5% CO_2, and fresh growth medium was added to the cells every 3–4 days until confluence. Cells were growth-arrested in serum-free medium for 48 h before use in experiments, and all experiments were performed under serum-free conditions unless otherwise stated. All experiments used cells at passages 6–8 and were performed on confluent cultures except for those experiments using antibody visualization, in which cells of ~70% confluence were used for optimal antibody coverage. Myofibroblasts were differentiated by incubation of fibroblast cultures in serum-free medium containing 10 ng/ml TGF-β1 for 72 h. For lipid raft disruption, fibroblast cultures were incubated in medium containing 50 μg/ml nystatin for 1 h prior to further experimentation. This was confirmed by using 10 μM methyl-β-cyclodextrin in place of nystatin. To inhibit EGFR signaling, 10 μM AG1478 was used for 1-h pretreatments before further experimentation. The HA-pericellular coat was removed by incubating 1 unit of *Streptomyces* hyaluronidase or 100 μg/ml bovine testicular hyaluronidase (positive control) with differentiated myofibroblasts for 1 h before sample analysis.

Laser Confocal Microscopy and Fluorescence Recovery after Photobleaching (FRAP)—Cells were grown to 70% confluence on 22-mm diameter glass coverslips in 35-mm dishes. Following appropriate experimental methods, the coverslip was removed from the medium and mounted on a heated microscope stage at 37 °C. 500 μl of medium was placed onto the mounted coverslip, and primary fluorophore-conjugated antibodies/ligands were added (rat monoclonal anti-CD44 FITC/phycoerythrin red-conjugated antibody (dilution 1:500; Abcam (Cambridge, UK)); mouse monoclonal anti-EGFR FITC-conjugated antibody (1:500 dilution; Abcam); cholera toxin subunit B TRITC conjugate (1:500 dilution; Invitrogen)). Analysis was performed by laser confocal microscopy and FRAP.

Co-localization data were analyzed using ImageJ (National Institutes of Health) and intensity correlation analysis, including the following statistical tests: Mander's co-localization coefficient (percentage of FITC co-localization with TRITC), Pearson's correlation coefficient (*Rr*) (where perfect correlation =

1); and the intensity correlation quotient (ICQ), where with random staining ICQ = ~0, and for dependent staining, 0 < ICQ ≤ +0.5 (36).

Leica confocal software (Leica Microsystems, Hamburg, Germany) was used to assess FRAP data and generate fluorescence intensity ratios (F_z/F_o, where F_z is the intensity of the photobleached zone and F_o is the intensity of the control region taken from outside of the photobleached zone). Average diffusion constants (D) were calculated from the equation, $D = (w^2/2t_{½})\gamma_D$, where w is the radius of the photobleached area, $t_{½}$ is the half-time of fluorescent recovery, and γ_D is a constant that is dependent on experimental conditions (37). Mobile fractions represent the fraction of receptors that had the ability to recover into the photobleached zone over the observed time.

Immunoprecipitation—Cells were grown to confluence in 35-mm dishes, and total cellular protein was extracted in radioimmune precipitation assay lysis buffer containing 1% protease inhibitor mixture, 1% PMSF, and 1% sodium orthovanadate (Santa Cruz Biotechnology, Inc.), as described previously (32). Cell protein samples were incubated with anti-EGFR antibody-conjugated Magnabind beads (Thermo Scientific Pierce) overnight at 4 °C. Following three washes with Nonidet P-40 buffer, the beads were resuspended in PBS and transferred to clean microcentrifuge tubes. The bead-antibody-protein complex was boiled with reducing buffer for 5 min before the supernatant was transferred into gel lanes for SDS-PAGE. Western blotting with rat anti-CD44 primary antibody was used for further analysis. The specificity of immunoprecipitation was confirmed by negative control reactions performed with mouse serum IgG.

Western Blot Analysis—Western blot analysis was used to assess expression of total and phosphorylated EGFR, CD44, total and phosphorylated ERK1 and ERK2 (p44/p42), total and phosphorylated CaMKII, total and phosphorylated Smad2, and TGF-βRI. Cells were grown to confluence in 35-mm dishes; total protein was extracted in radioimmune precipitation assay lysis buffer containing 1% protease inhibitor mixture, 1% PMSF, and 1% sodium orthovanadate (Santa Cruz Biotechnology, Inc.). Western blot analysis was carried out as described in our previous work (32). The nitrocellulose membranes were incubated with the appropriate primary antibodies in 1% BSA, 0.1% Tween-PBS. Where necessary, expression of GAPDH was analyzed as a control to ensure equal loading (rabbit anti-GAPDH; 1:5000 dilution). The secondary antibodies used were anti-mouse IgG/horseradish peroxidase conjugate (Abcam) (1:5000 dilution in 1% BSA, 0.1% Tween-PBS), anti-rabbit IgG/horseradish peroxidase conjugate (Cell Signaling Technology, Beverly, MA) (1:5000 dilution in 1% BSA, 0.1% Tween-PBS), and anti-rat IgG/horseradish peroxidase conjugate (Santa Cruz Biotechnology, Inc.) (1:5000 dilution in 1% BSA, 0.1% Tween-PBS). Detection was performed using ECL reagent (GE Healthcare).

siRNA Transfection—Transient transfection of fibroblasts was performed with specific siRNA nucleotides targeting CD44 (ID 4390824, Applied Biosystems) and HAS2 (ID 4392420, Applied Biosystems). Transfection was performed in 35-mm dishes using Lipofectamine 2000 transfection reagent (Invitrogen) in accordance with the manufacturer's protocol as described in our previous work (32). As a control, cells were transfected with negative control siRNA (a scrambled sequence that bore no homology to the human genome) (Applied Biosystems).

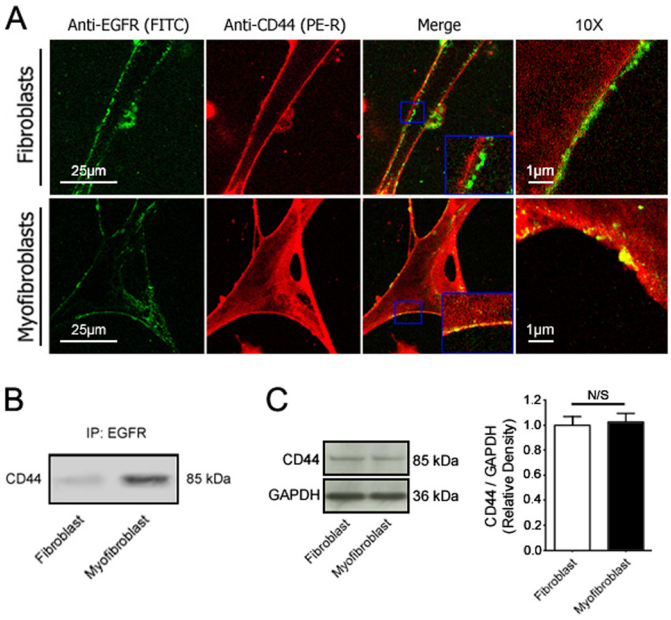

FIGURE 1. **EGFR and CD44 co-localization following myofibroblast differentiation.** *A*, cells were grown to 70% confluent monolayers and were growth-arrested for 48 h. Cells were then incubated in serum-free medium alone (fibroblasts) or in medium containing 10 ng/ml TGF-β1 for 72 h (myofibroblasts). The expression of EGFR (*green*; FITC) and CD44 (*red*; phycoerythrin red (*PE-R*)) was examined by confocal laser microscopy; areas of co-localization are shown in the *merged images* (*yellow*; *enlarged images* shown in *blue boxes*). Images shown are a representation of five independent experiments. Original magnification was ×630. *B*, co-localization of EGFR and CD44 was analyzed by immunoprecipitation (*IP*) for EGFR followed by immunoblotting for CD44. The image shown is representative of three individual experiments. *C*, Western blot analysis of total CD44 protein in fibroblasts and myofibroblasts. GAPDH was used as a loading control. A representative blot is shown. The densitometry graph shown represents mean ± S.E. (*error bars*) of three individual experiments. *N/S*, no significance.

Reverse Transcription (RT) and Real-time QPCR—RT and real-time QPCR were used to assess α-SMA, CD44, and HAS2 mRNA expression in fibroblasts or myofibroblasts. The cells were grown in 35-mm dishes and washed with PBS prior to lysis with TRI Reagent solution (Ambion) and RNA purification according to the manufacturer's protocol. Reverse transcription was performed using high capacity cDNA reverse transcription kits according to the manufacturer's protocol (Applied Biosystems). This uses the random primer method for initiating cDNA synthesis. As a negative control, RT was performed with sterile H_2O replacing the RNA sample. QPCR was performed as in our previous studies (32) using the 7900HT Fast Real Time PCR System (Applied Biosystems).

Biochemical Isolation of Lipid Rafts—All procedures were carried out on ice. Fibroblast or myofibroblasts monolayers were washed twice with ice-cold PBS, and cells from two 35-mm confluent dishes were then scraped into 1 ml of ice-cold lysis buffer containing 1% Triton X-100 and 1% protease inhibitor mixture (Sigma-Aldrich). Samples were vortexed thoroughly and left to incubate on ice for 30 min before centrifugation (1500 × *g* for 5 min at 4 °C). The sample supernatants were placed at the bottom of a 5-ml ultracentrifuge tube. Discontinuous OptiPrep gradients (35–20% and 0%) (Sigma-Aldrich)

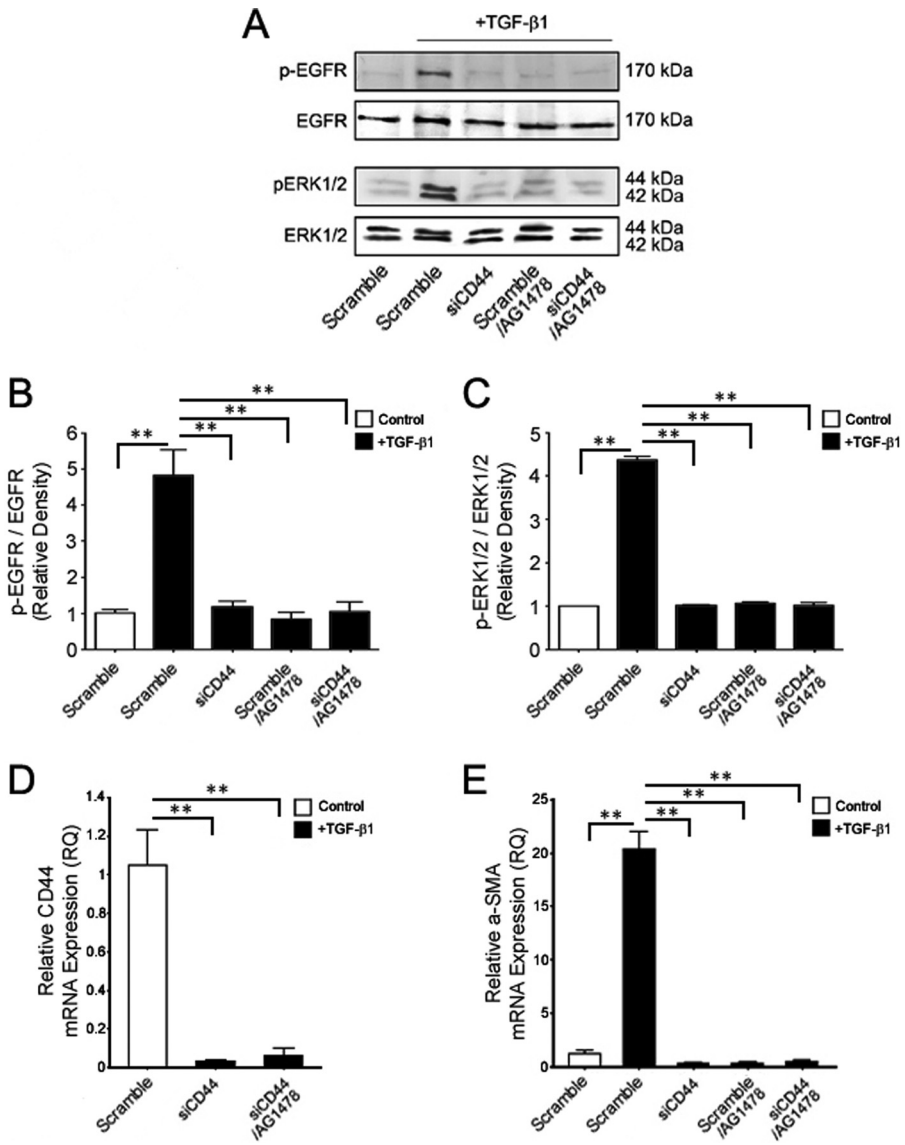

FIGURE 2. **The effect of EGFR and CD44 expression and signaling on cellular phenotype.** *A*, fibroblasts were transfected with a scrambled siRNA sequence or siRNA targeting CD44 prior to treatments with or without AG1478 for 1 h before TGF-β1 for 72 h. Phosphorylation of EGFR and ERK1/2 was analyzed by Western blotting. Total EGFR and ERK1/2 proteins were used as loading controls. The image shown is representative of three independent experiments. *B*, densitometric analysis of phosphorylated EGFR (*p-EGFR*) normalized to total EGFR. The graph shows results ± S.E. (*error bars*) of three independent experiments. *C*, densitometric analysis of phosphorylated ERK1/2 (*p-ERK1/2*) normalized to total ERK1/2. The graph shows mean ± S.E. of three independent experiments. *D*, QPCR was used to confirm CD44 mRNA knockdown by siCD44. Results shown are mean ± S.E. of three individual experiments. *E*, QPCR was used to analyze α-SMA mRNA following siCD44 and AG1478 cellular treatments. Results shown are mean ± S.E. of three individual experiments. **, $p < 0.01$.

were made according to the manufacturer's protocol and added to the ultracentrifuge tube containing the sample by overlaying. The gradients were centrifuged at 200,000 × *g* for 14 h with 2 h of gentle acceleration and deceleration on either side in an Optima-Max ultracentrifuge (Beckman Coulter). Centrifugation time was sufficient to gain a continuous gradient, from which 10 500-μl fractions were carefully collected, starting from the top of each tube.

Fraction Analysis—The collected fractions were subjected to SDS-PAGE and transferred to a nitrocellulose membrane for Western blot analysis as described above. The presence of proteins of interest was examined by specific antibodies. The presence of caveolin-1 (Cav-1) and EEA-1 were used to determine whether the fraction represented lipid raft or non-raft proteins, respectively. Following transfer of proteins to the nitrocellulose membrane, the membrane was blocked with 5% nonfat powdered milk in 0.5% Tween-PBS for 1 h and then incubated with rabbit anti-Cav-1 (dilution 1:500; Sigma-Aldrich) or mouse anti-EEA-1 (dilution 1:5000; Cell Signaling Technology) in 1% BSA, 0.1% Tween-PBS at 4 °C overnight. The blots were subsequently washed with 0.1% Tween-PBS and then incubated with the appropriate secondary antibody and visualized using ECL reagent (GE Healthcare). Cholera toxin subunit B-HRP conjugate (CTX-HRP) (dilution 1:500; Sigma-Aldrich) was incubated with cell monolayers on ice for 1 h prior to lysis. CTX-HRP-bound samples were used for dot blot analysis to confirm the presence of lipid rafts. 5 μl of each fraction was pipetted onto a prewashed nitrocellulose membrane and allowed to dry, and the membrane was washed briefly with PBS and visualized with ECL reagent (GE Healthcare).

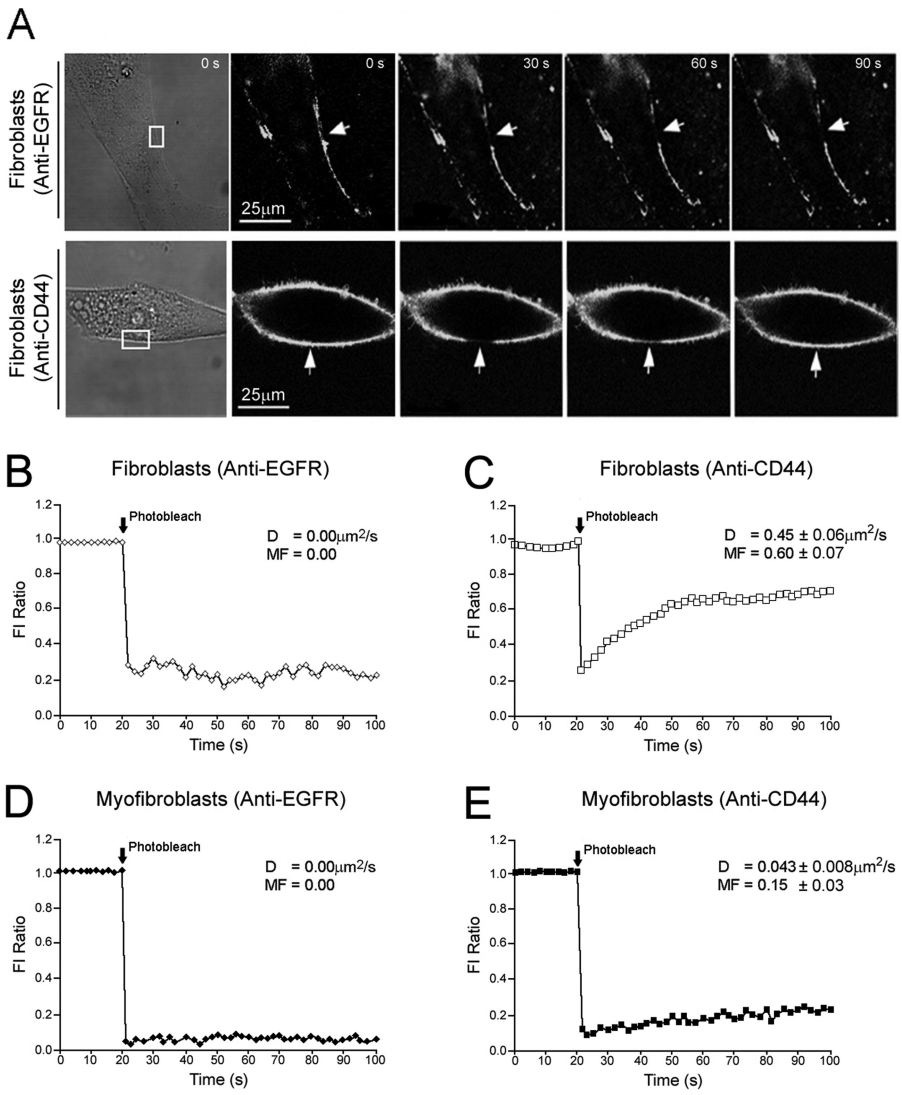

FIGURE 3. **Mobility of EGFR and CD44 in fibroblasts and myofibroblasts.** *A*, sample time lapse series of FRAP experiments. Original magnification was ×630. Fibroblasts or myofibroblasts were grown to 70% confluent monolayers on 22-mm diameter glass coverslips in 35-mm 6-well tissue culture plates. Cells were growth-arrested in serum-free medium for 48 h. FRAP was performed at 37 °C by photobleaching an ~10-μm area of the cell membrane (indicated by *white boxes* on the *bright field images*). The recovery of fluorescence into this area (indicated by *white arrows*) was quantified and expressed as a fraction of the fluorescence intensity (*FI*) of a second region of membrane outside of the photobleached area (*FI Ratio*). Complete quantified time courses, average diffusion constants (*D*), and mobile fractions (*MF*) are shown for EGFR in fibroblasts (*B*), CD44 in fibroblasts (*C*), EGFR in myofibroblasts (*D*), and CD44 in myofibroblasts (*E*). All results shown are representative of five independent experiments. Statistics shown are mean ± S.E. (*error bars*) of five independent experiments.

Flow Cytometry—Fibroblasts were grown to confluence and growth-arrested in serum-free medium for 48 h before treatment with serum-free medium alone or serum-free medium containing 10 ng/ml TGF-β1 for 72 h. Where necessary, cells were pretreated with 50 μg/ml nystatin for 1 h. Cells were washed with PBS and incubated with 0.01% trypsin-EDTA to lift the cells. Trypsin was subsequently neutralized with FCS, and the cell solution was centrifuged at 1500 × *g* for 5 min at 20 °C. The supernatant was aspirated, and the cell pellet was resuspended in 1% BSA-PBS containing rabbit anti-Cav-1 antibody (1:10,000) (Sigma-Aldrich), followed by 30 min of incubation with 1% BSA-PBS containing anti-rabbit-FITC (1:10,000) (Calbiochem) on ice, before further washes and resuspension. Flow cytometry was performed using a FACSCanto II flow cytometer (BD Biosciences), and data were analyzed using FlowJo version 7 (Tree Star).

Immunocytochemistry—Cells were grown to 70% confluence in 8-well glass chamber slides. The culture medium was removed, and the cells were washed with sterile PBS prior to fixation in 4% paraformaldehyde for 10 min at room temperature. To ensure visualization of cytoskeletal proteins, fixed slides were permeabilized with 0.1% Triton X-100 in PBS for 10 min when necessary. Slides were washed with PBS and then blocked with 1% BSA for 30 min prior to a further washing step. Subsequently, the slides were incubated with the primary antibody diluted in 0.1% BSA-PBS overnight at 4 °C (rat monoclonal anti-CD44 antibody (A020, 1:200 dilution; Calbiochem), monoclonal mouse anti-EGFR antibody (GR01, 1:30 dilution; Calbiochem), and monoclonal mouse anti-α-SMA antibody (1:25 dilution; DAKO, Aachen, Germany)). Following a further wash step, slides were incubated with secondary antibodies for 1 h at room temperature in darkness (anti-mouse IgG/AlexaFluor 488 and anti-rat

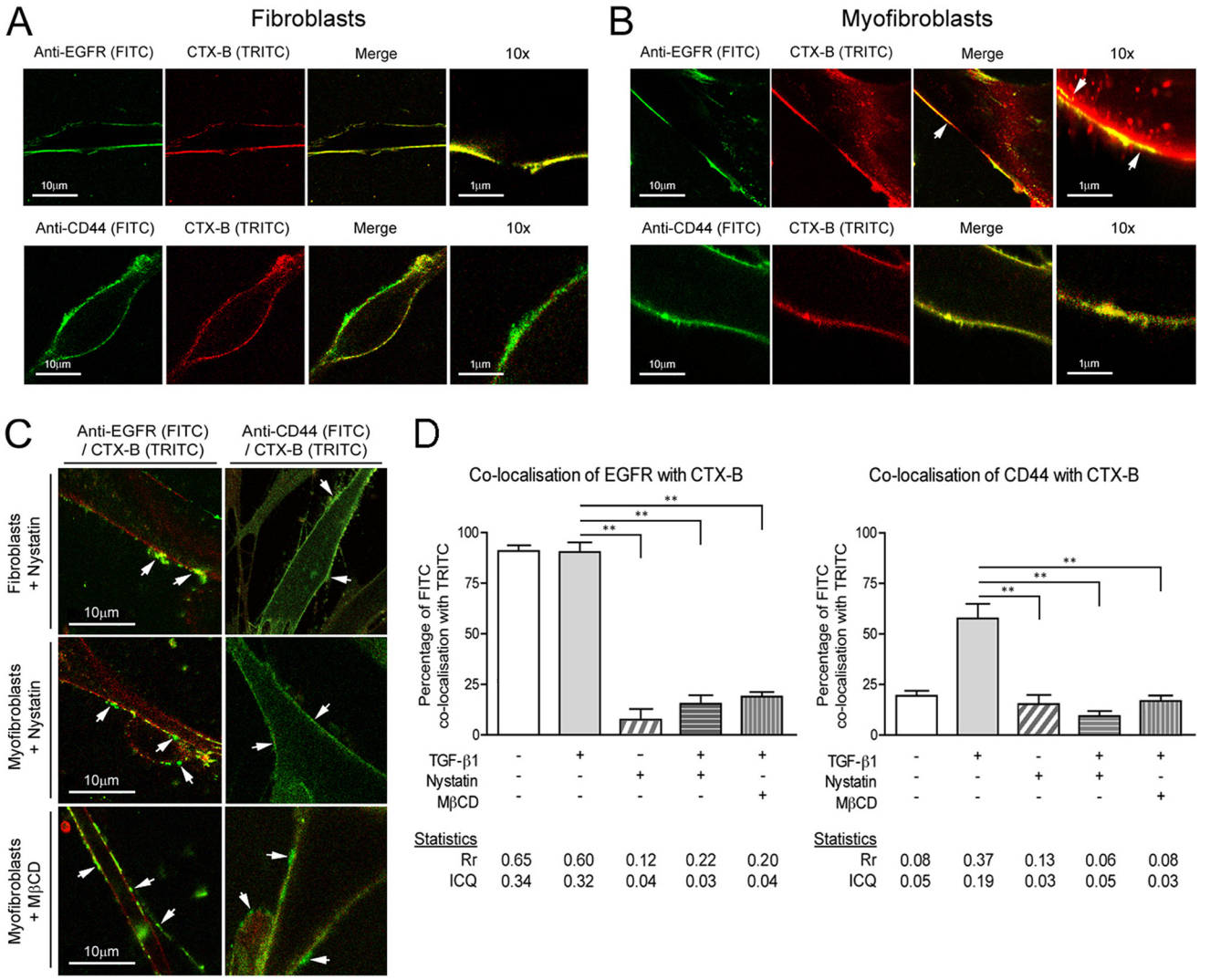

FIGURE 4. **EGFR is associated with cholesterol-rich lipid raft domains of the cell membrane.** Fibroblasts or myofibroblasts were grown to 70% confluent monolayers on 22-mm diameter glass coverslips in 35-mm 6-well tissue culture plates. Cells were growth-arrested in serum-free medium for 48 h before mounting onto a heated stage (37 °C), and 500 μl of fresh medium was applied for complete cell coverage. The expression of EGFR (*green*; FITC) and CTX-B binding (*red*; TRITC) (*A*) and CD44 (*green*; FITC) and CTX-B binding (*red*; TRITC) (*B*) was examined by confocal laser microscopy; areas of co-localization are shown in the *merged images* (*yellow*). Areas of CTX-B binding with EGFR are marked by *white arrows*. Sample images shown are representative of five individual experiments. Original magnification was ×630. *C*, cells were pretreated with nystatin (50 μg/ml) or methyl-β-cyclodextrin (*MβCD*) (10 mM) for 1 h prior to incubation with serum-free medium alone (fibroblasts) or serum-free medium containing TGF-β1 (10 ng/ml) for 72 h (myofibroblasts). Cells were then examined by confocal laser microscopy for EGFR or CD44 expression (*green*; FITC) and CTX-B binding (*red*; TRITC). *White arrows* indicate areas of EGFR or CD44 expression without CTX-B binding. Images shown are representative of three individual experiments. Original magnification was ×630. *D*, graphs displaying the percentage of co-localization of FITC (EGFR/CD44) with TRITC (CTX-B) (Mander's co-localization coefficient). Statistical analysis includes the average Pearson's correlation coefficient (*Rr*) and the ICQ for each experimental condition. Results shown are mean ± S.E. of three independent experiments. **, $p < 0.01$.

IgG/AlexaFluor 555; Invitrogen, Paisley, UK). Cells were then mounted and analyzed by fluorescent microscopy.

Statistical Analysis—Western blot images were densitometrically analyzed by ImageJ (National Institutes of Health). Graphical data are expressed as averages ± S.E. The unpaired two-tailed Student's *t* test was used to identify statistical significance. Data were analyzed using the software MiniTab version 15.0 (MiniTab Solutions). Significance was as follows: *, $p < 0.05$; **, $p < 0.01$.

RESULTS

TGF-β1-dependent Differentiation in Fibroblasts Is Mediated through the HA Receptor, CD44, and Its Co-localization with EGFR—Expression of EGFR and CD44 in fibroblasts and the changes associated with TGF-β1-dependent differentiation were assessed by confocal laser scanning microscopy (Fig. 1*A*). Both receptors were expressed in fibroblasts with strong independent staining along the cell membrane. Following TGF-β1-induced differentiation to myofibroblasts, however, CD44 (*red*) expression was found in areas of co-localization with EGFR (*green*) visible as *yellow* (*merged*). Following lysis of myofibroblasts, CD44 was found to co-immunoprecipitate with EGFR (Fig. 1*B*). Potential changes in the expression of total CD44 receptor protein were examined, and no significant changes were found (Fig. 1*C*). Both transfection of siRNA, targeting CD44 (siCD44), and treatment with the chemical inhibitor of EGFR activation, AG1748, inhibited phosphorylation of EGFR and of the downstream signaling proteins, ERK1/2 (Fig. 2, *A–C*). CD44 knockdown was confirmed by QPCR (Fig. 2*D*), and the affect of each treatment on differentiation was assessed by

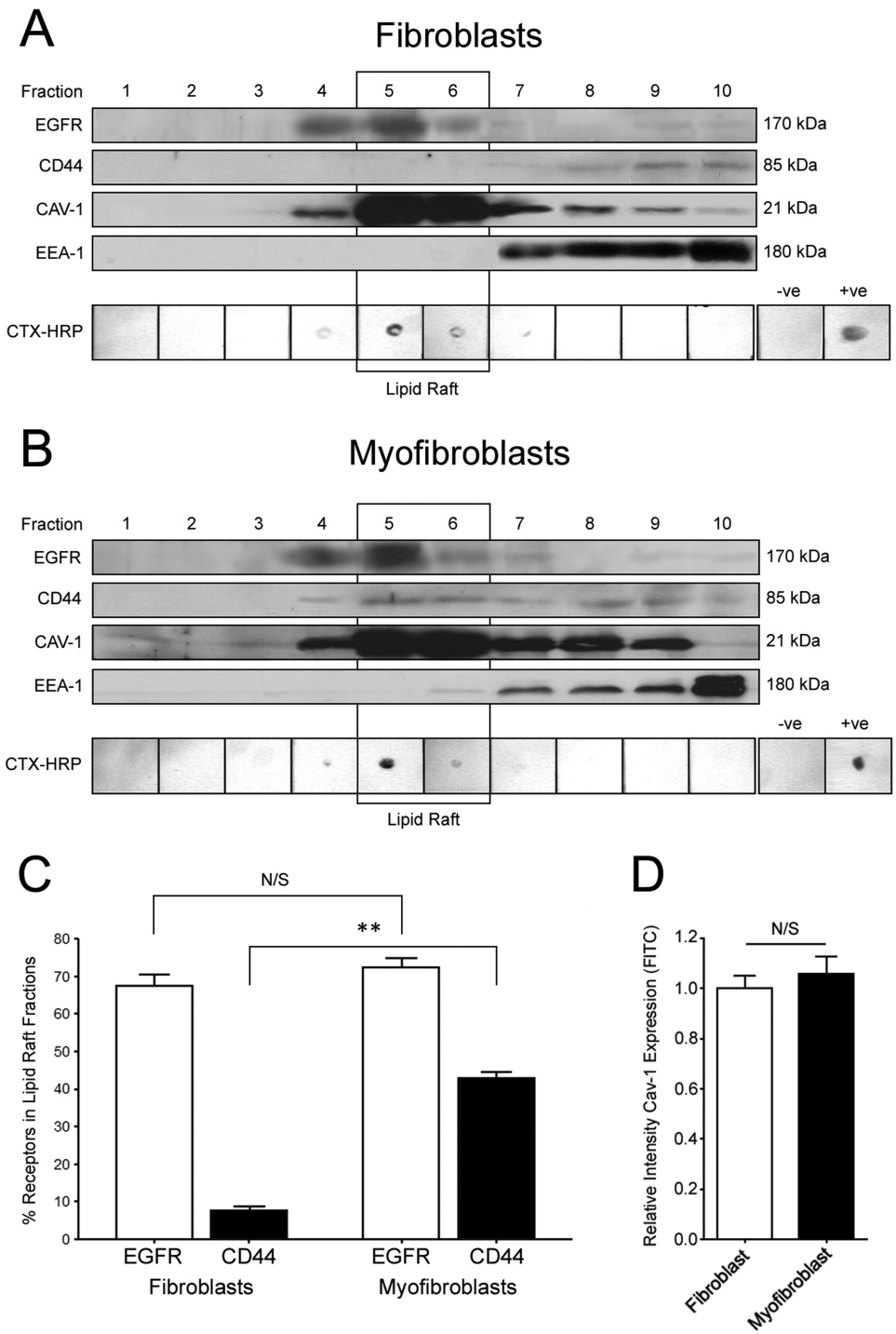

FIGURE 5. **EGFR is found in fractions positive for Cav-1 and CTX and in fractions containing CD44 following cellular differentiation.** Cells were grown to confluence and were growth-arrested for 48 h. Cells were incubated in serum-free medium alone (fibroblasts) (*A*) or serum-free medium containing 10 ng/ml TGF-β1 (*B*) for 72 h (myofibroblasts). Cellular membrane preparations were separated in a discontinuous OptiPrep gradient by ultracentrifugation. Fractions were analyzed for the presence of EGFR and CD44. Cav-1 was used to detect fractions positive for lipid rafts, and EEA-1 was used for non-raft fractions. Lipid raft fractions were confirmed using CTX-HRP dot blots for each fraction. Positive and negative control dot blots were used to confirm the specificity of CTX-HRP. *C*, quantification of the percentage of EGFR and CD44 found within lipid raft fractions 5 and 6 in fibroblasts and myofibroblasts. Results shown are mean ± S.E. (*error bars*) of three independent experiments. *D*, flow cytometry analysis of cell surface expression of Cav-1 in fibroblasts and myofibroblasts. Unlabeled cells were used as intensity controls. The bar graph of relative intensity shown represents mean ± S.E. of three individual experiments. *N/S*, no significance; **, $p < 0.01$.

QPCR (Fig. 2*E*). These data highlight the importance of both EGFR and CD44 and their active roles in the differentiation and signaling response.

FRAP was used to investigate receptor dynamics in the plasma membrane of fibroblasts and myofibroblasts (Fig. 3). In fibroblasts, EGFR was bound in clusters within discrete areas of the cell membrane (Fig. 3*A*) and did not diffuse into the bleached zone (Fig. 3*B*). CD44, however, diffused rapidly (<100 s) into the area of bleaching (Fig. 3, *A* and *C*). In myofibroblasts, EGFR was also found in static membrane domains (Fig. 3*D*). In

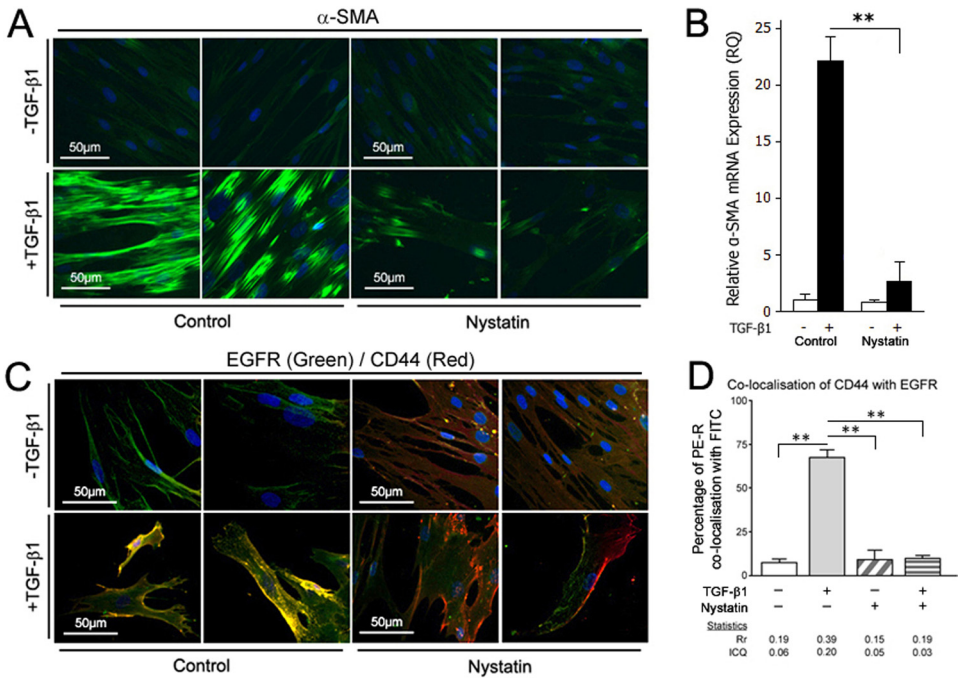

FIGURE 6. **Lipid raft disruption prevents EGFR and CD44 co-localization and myofibroblast differentiation.** Cells were grown to 70% confluent monolayers and were growth-arrested for 48 h. Cells were incubated with 50 μg/ml nystatin for 1 h before incubation in serum-free medium alone (fibroblasts) or medium containing 10 ng/ml TGF-β1 for 72 h (myofibroblasts). *A*, α-SMA expression (*green*) was examined by immunocytochemistry. Hoechst staining was used to visualize nuclei (*blue*). Naive IgG was used for negative controls. Results shown are representative of three independent experiments. Original magnification was ×400. *B*, untreated and nystatin-treated cells were incubated in serum-free medium alone or with serum-free medium containing 10 ng/ml TGF-β1 for 72 h before mRNA was extracted and quantified for α-SMA by QPCR. Results are mean ± S.E. (*error bars*) of three individual experiments. *C*, EGFR (*green*) and CD44 (*red*) expression was examined by immunocytochemistry. *Merged images* (*yellow*) show areas of co-localization. Hoechst staining was used to visualize nuclei (*blue*). Naive IgG was used for negative controls. Images shown are representative of five individual experiments. Original magnification was ×400. *D*, graphs displaying the percentage of co-localization of phycoerythrin red (*PE-R*) (CD44) with FITC (EGFR) (Mander's co-localization coefficient). Statistical analysis includes the average Pearson's correlation coefficient (*Rr*) and ICQ for each experimental condition. Results shown are mean ± S.E. of five individual experiments. **, $p < 0.01$.

contrast to fibroblasts, however, CD44 on the surface of myofibroblasts had a reduced mobility, with a diffusion constant of only 10% of that in fibroblasts (Fig. 3*E*). The mobile fraction of CD44 receptors was also reduced from ~60% in fibroblasts to 15% in myofibroblasts. These results suggest that the loss of CD44 mobility in the membrane may be an important factor in the mechanism of myofibroblast induction.

EGFR Is Localized to Cholesterol-rich Membrane-bound Lipid Raft Domains in Fibroblasts, and Co-localization with CD44 at These Domains Is Necessary for Differentiation—EGFR has been found previously in lipid rafts in tumor cells and neuronal cells (38, 39). To investigate whether it was also located in rafts in primary human fibroblasts, we used laser confocal microscopy with the cholera toxin subunit-B (CTX-B)-TRITC conjugate, which binds GM1-containing, cholesterol-rich regions of the cell membrane (Fig. 4). Fig. 4*A* indicates that in fibroblasts, wherever EGFR was located, there were also cholesterol-rich domains containing CTX-B (*yellow merged images*). In contrast, CTX-B and CD44 had large areas of no co-localization with a few discrete areas of co-localization observed, as can be seen in the *merged images*. In myofibroblasts (Fig. 4*B*), there was also co-localization of EGFR with CTX-B at the cell surface, although EGFR binding was not exclusively found in all areas positive for CTX-B (*white arrows*). In contrast to fibroblasts, however, CD44 on myofibroblasts was highly co-localized to areas positive for CTX-B (*merged panel*).

To confirm the involvement of lipid rafts, both nystatin and methyl-β-cyclodextrin were used independently (Fig. 4*C*) to disrupt rafts. Following incubation of myofibroblasts with either compound, the co-localization of both EGFR and CD44 with CTX-B was reduced. EGFR or CD44 expression was visible in areas devoid of CTX-B binding (indicated by *white arrows*). A summary of results from three independent experiments showing the degree of co-localization and the ICQ is shown in Fig. 4*D*. These data indicate that there was a 4–5-fold decrease in EGFR association with CTX-B following nystatin treatment before the addition of TGF-β1. They also demonstrate a 3-fold increase in CD44 association with CTX-B following myofibroblastic induction with TGF-β1, which is lost in cells pretreated with nystatin.

To further test the hypothesis that lipid rafts serve as the primary location of EGFR and co-localization with CD44 following differentiation, lipid rafts were biochemically isolated by ultracentrifugation, and the collected fractions were examined for the lipid raft markers Cav-1 and CTX-HRP. EEA-1 was used to determine non-raft regions of the cell membrane. In fibroblasts, EGFR was primarily found in lipid raft domains (Cav-1/CTXB-positive fractions; fraction 5 and 6) and CD44 in non-raft regions (EEA-1-positive fractions; fractions 8–10) (Fig. 5*A*). In differentiated myofibroblasts, a proportion of CD44 was found to move into the fractions positive for lipid raft markers, demonstrating that CD44 existed in two populations, within and outside lipid raft regions (Fig. 5*B*). The quantification of

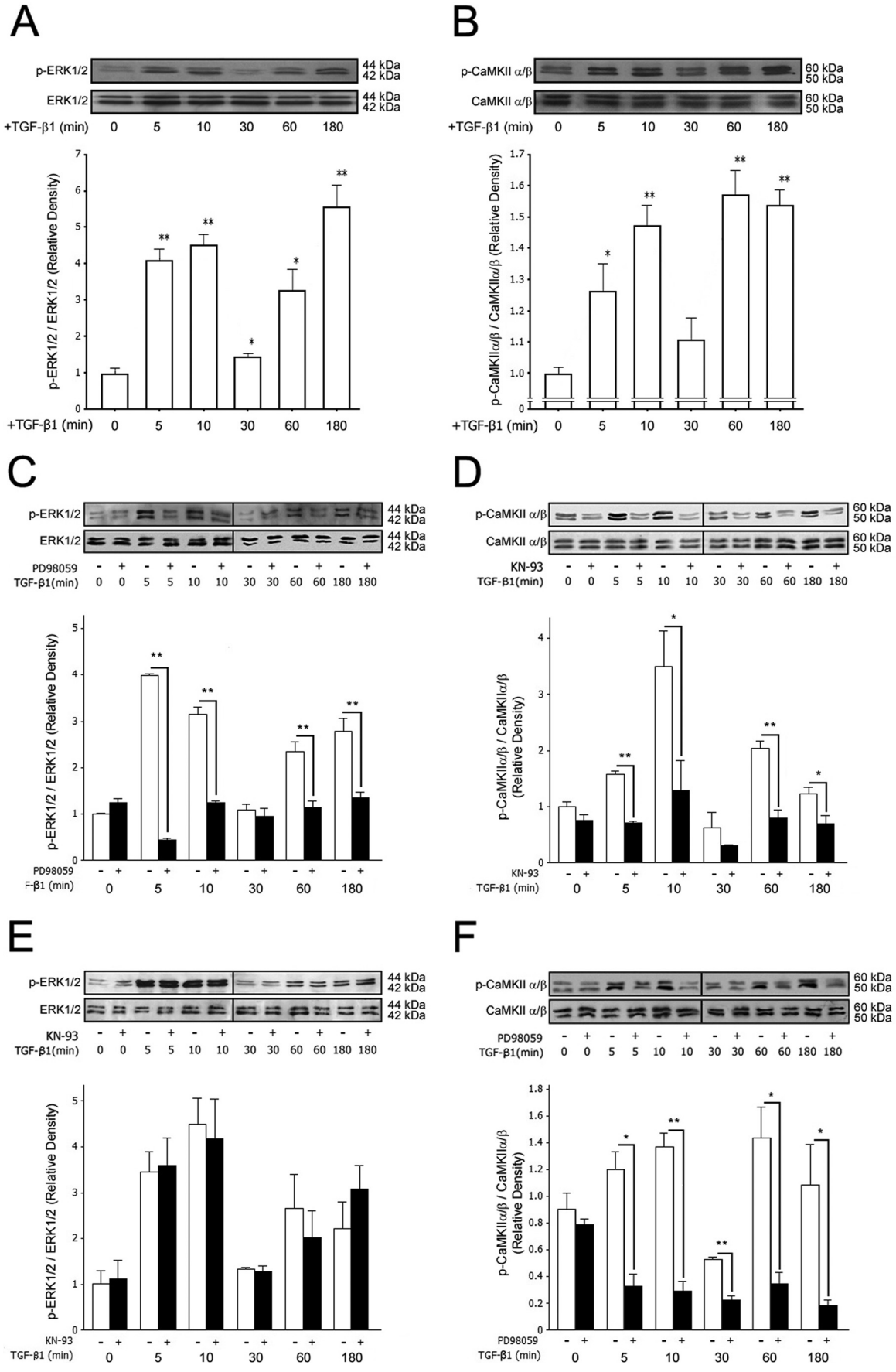
A
p-ERK1/2
ERK1/2
44 kDa
42 kDa
+TGF-β1 (min) 0 5 10 30 60 180
p-ERK1/2 / ERK1/2 (Relative Density)
B
p-CaMKII α/β
CaMKII α/β
60 kDa
50 kDa
p-CaMKIIα/β / CaMKIIα/β (Relative Density)
C
PD98059
TGF-β1(min) 0 0 5 5 10 10 30 30 60 60 180 180
D
KN-93
E
KN-93
F
PD98059

receptors in lipid raft fractions (Fig. 5*C*) indicated that the quantity of EGFR found in lipid raft fractions did not alter significantly between cellular phenotypes. The presence of CD44 in lipid raft fractions significantly increased from ~10% to more than 40% following differentiation. Cellular expression of Cav-1 (Fig. 5*D*) had no significant change between fibroblasts and myofibroblasts, signifying that the increase of CD44 directed toward lipid raft fractions was a primary change as a result of differentiation and not a consequence of an increased generation of Cav-1-positive rafts.

To investigate the degree to which lipid rafts were involved in the mechanism controlling myofibroblast induction, α-SMA expression was assessed by immunocytochemistry (Fig. 6*A*). α-SMA was markedly down-regulated in cells pretreated with nystatin. QPCR (Fig. 6*B*) demonstrated that this was also a transcriptional effect on α-SMA mRNA. Co-localization of EGFR and CD44 in fibroblasts pretreated with nystatin before the induction of differentiation with TGF-β1 was prevented, indicating that lipid rafts were key locations of the EGFR-CD44 association (Fig. 6*C*). Statistical analysis showed a decrease in CD44 co-localization with EGFR in myofibroblasts from 70% to ~10% if cells were pretreated with nystatin (Fig. 6*D*). Flow cytometry and Western blot analysis showed that nystatin treatment did not alter the expression or total protein levels of either EGFR or CD44 (data not shown). These results support the importance of lipid rafts in the TGF-β1-dependent differentiation pathway.

TGF-β1 Induces ERK and CaMKII Phosphorylation—Previous research has shown that mitogen-activated protein kinases 1 and 2 (ERK1/2) are involved in the differentiation and proliferation of various cell types (33, 40–43). Western blotting was used to assess the degree of phosphorylation of these kinases following incubation with TGF-β1 (Fig. 7, *A* and *B*). Fig. 7*A* shows the characteristic biphasic phosphorylation of ERK1/2, peaking at 10 min and again at 3 h after the addition of TGF-β1.

CaMKII is a kinase that is involved in cytoskeletal remodeling and the differentiation response (44, 45). Western blotting for phosphorylated CaMKII (Fig. 7*B*) showed that CaMKII was also activated, and its phosphorylation had a biphasic time-dependent activation similar to ERK phosphorylation, implicating CaMKII in the TGF-β1-dependent signaling pathways involved in myofibroblast differentiation. Both ERK1/2 and CaMKII phosphorylation did not fluctuate over the 3 h if cells remained in serum-free conditions (data not shown).

We next examined whether ERK and CaMKII activation were independent of each other using the chemical inhibitor of ERK phosphorylation, PD98059, and the chemical inhibitor of CaMKII, KN-93. PD98059 inhibited ERK activation (Fig. 7*C*) following TGF-β1 stimulation, attenuating both peaks of the biphasic activation profile. Similarly, KN-93 attenuated both peaks of CaMKII activation (Fig. 7*D*) as expected. In addition, KN-93 had no effect on ERK1/2 signaling, and the biphasic activation was retained (Fig. 7*E*). Interestingly, PD98059 inhibited CaMKII phosphorylation (Fig. 7*F*), suggesting that ERK activation was a necessary upstream mediator of CaMKII activation. Because CaMKII activation was abolished following incubation with the chemical inhibitor of ERK1/2, the results shown here suggest that following the addition of TGF-β1, ERK is activated first, leading to the downstream activation of CaMKII.

EGFR-CD44 Co-localization in Lipid Rafts Is Responsible for Early Differentiation Signaling, and Disruption of Lipid Rafts Inhibits the Early Signaling of the EGFR-ERK1/2-CaMKII Pathway—To confirm that it was raft-associated co-localization that was responsible for the induction of ERK and CaMKII, nystatin was used to disrupt lipid rafts, and then Western blotting was used to examine the phosphorylation of EGFR, ERK1/2, and CaMKII (Fig. 8). Nystatin inhibited the early signaling phase of TGF-β1-dependent EGFR (Fig. 8*A*), ERK (Fig. 8*B*), and CaMKII (Fig. 8*C*) phosphorylation without affecting the late activation phase of either kinase. The loss of the early ERK and CaMKII signaling phases and the fibroblast resistance to differentiation following nystatin treatment confirmed that the early signaling phase was primarily responsible for the initiation of fibroblast to myofibroblast differentiation, as reported previously (33), and that it was initiated in lipid rafts. Additionally, the expression of TGF-βRI and the activation of the Smad2 pathway remained unaffected by nystatin treatment (data not shown).

HAS2-regulated HA Synthesis Is a Key Mediator of TGF-β1-dependent Myofibroblast Differentiation and Proliferation—HAS2 is the enzyme primarily responsible for up-regulation of HA synthesis in fibroblasts following TGF-β1-induced differentiation to myofibroblasts (22–25). We have previously shown that HAS2 is an important mediator of differentiation in fibroblasts (32, 33). Here we confirm that transfection with siRNA targeting HAS2 (siHAS2) was sufficient to knock down HAS2 mRNA expression (Fig. 9*A*) and prevent α-SMA up-regulation (Fig. 9*B*). CD44 co-immunoprecipitation with EGFR was also prevented following siHAS2 transfection (Fig. 9*C*). We sought to determine whether HA production by HAS2 was a direct regulator of the ERK and CaMKII intracellular signaling pathways leading to phenotypic change. Cells were transfected with siHAS2 or scrambled siRNA, and protein phosphorylation was assessed by Western blotting. When stimulated with TGF-β1, the fibroblasts transfected with siHAS2 had attenuation of

FIGURE 7. **TGF-β1 induces phosphorylation of both ERK and CaMKII, and ERK phosphorylation is an upstream regulator of CaMKII phosphorylation.** Confluent monolayers of fibroblasts were growth-arrested in serum-free medium for 48 h. Subsequently, they were incubated with 10 ng/ml TGF-β1 for up to 3 h, and phosphorylation of ERK1/2 (*A*) and CaMKII (*B*) proteins was assessed by Western blot analysis at the indicated times. Western blot analysis for the appropriate total proteins was performed to ensure equal loading of protein samples. Following scanning densitometry, phosphorylated ERK1/2 and CaMKII expression was corrected for the expression of total ERK1/2 and CaMKII protein, respectively, and is shown as mean ± S.E. of three separate experiments. Cells were incubated with 10 μM MEK/ERK inhibitor PD98059 (+) or left untreated (−) (*C* and *F*) or incubated with 10 μM CaMKII inhibitor KN-93 (+) with the inactive isomer KN-92 (−) as a control (*D* and *E*) for 1 h before incubation with 10 ng/ml TGF-β1 for up to 3 h. Phosphorylation of ERK1/2 (*C* and *E*) and CaMKII (*D* and *F*) proteins was assessed by Western blot analysis at the indicated times. Western blot analysis for the appropriate total proteins was performed to ensure equal loading of protein samples. Following scanning densitometry, alteration in phosphorylated ERK1/2 and CaMKII expression was corrected for the expression of total ERK1/2 and CaMKII protein, respectively. Representative blots of three independent experiments are shown, and densitometry graphs show mean ± S.E. of three separate experiments. *, $p < 0.05$; **, $p < 0.01$.

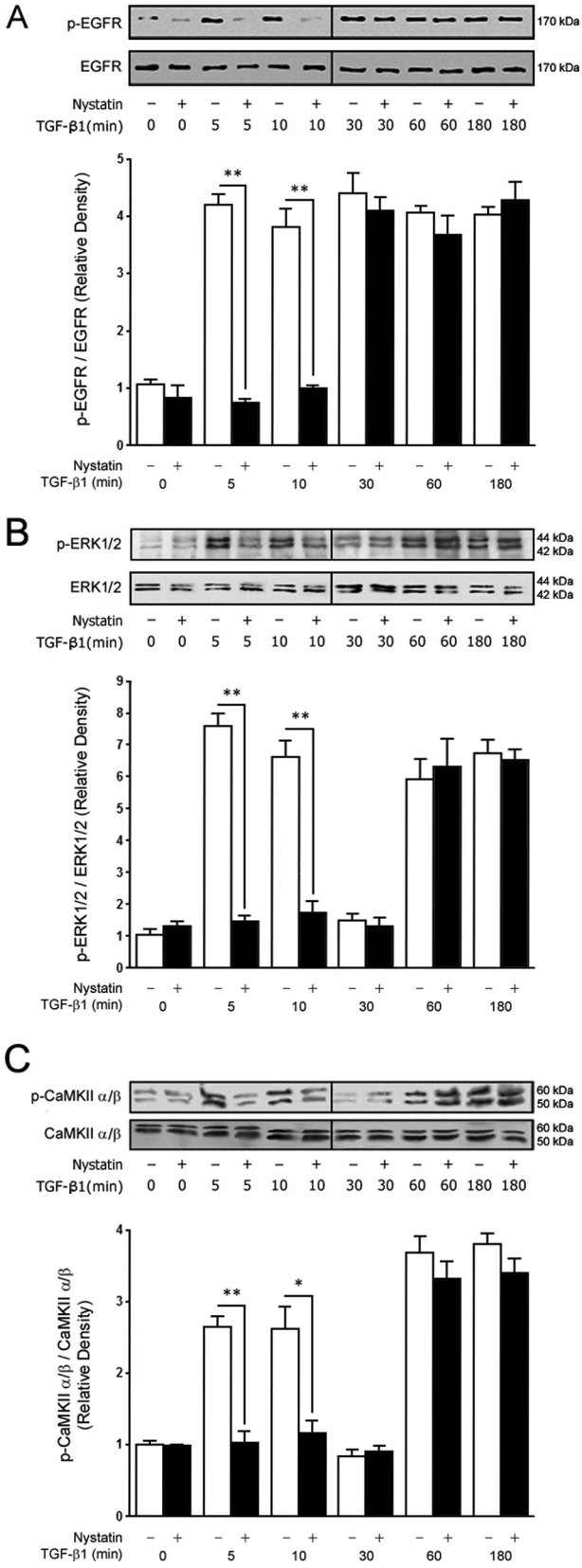

FIGURE 8. **Disruption of lipid rafts inhibits early EGFR, ERK, and CaMKII phosphorylation.** Confluent monolayers of fibroblasts were growth-arrested in serum-free medium for 48 h. Subsequently, cells were incubated with (+) or without (−) 50 μg/ml nystatin for 1 h before incubation with 10 ng/ml TGF-β1 for up to 3 h. *A*, phosphorylation of EGFR (*p-EGFR*) was assessed by Western blot analysis at the indicated times. Western blot analysis for total EGFR protein was performed to ensure equal loading of protein samples. The densitometry graph shows mean ± S.E. of three individual experiments. *B*, phosphorylation of ERK1/2 (*p-ERK1/2*) was assessed. Western blot analysis for total ERK1/2 protein was performed to ensure equal loading of protein samples. The densitometry graph shows mean ± S.E. (*error bars*) of three individual experiments. *C*, phosphorylation of CaMKII (*p-CaMKII*) was assessed. Western blot analysis for total CaMKII protein was performed to ensure equal loading of protein samples. The densitometry graph shows mean ± S.E. of three individual experiments. All blots shown are representative of three separate experiments. *, $p < 0.05$; **, $p < 0.01$.

EGFR (Fig. 9*D*), ERK (Fig. 9*E*), and CaMKII (Fig. 9*F*) activation. In addition, both the early and late peaks of the biphasic signaling pattern were lost. The loss of early ERK and CaMKII phosphorylation peaks supports previous studies, which have shown that HAS2 impairment in aged cells inhibits fibroblast differentiation (32). In addition, the attenuation of the late phosphorylation peaks supports previous findings highlighting HAS2 and HA as necessary mediators of fibroblast proliferation (33). To determine whether cell surface HA was necessary for CD44 co-localization with EGFR and membrane dynamics and behavior, confocal microscopy and FRAP analysis were used following hyaluronidase treatment (Fig. 10). Interestingly, CD44 co-localization with EGFR was partially lost following hyaluronidase treatment (Fig. 10, *A* and *B*). CD44 movement was restored in myofibroblasts incubated with hyaluronidase from both *Streptomyces* (*S*) and bovine testicular (*BT*) sources (Fig. 10, *C–E*); however, the mobile fraction indicated that hyaluronidase alone was not sufficient to restore mobility to the levels observed in fibroblasts. These data suggest that HAS2 production of the HA-pericellular coat was partly responsible for the sequestration and anchoring of CD44 into lipid raft domains, where it co-localizes with EGFR and enables the resulting differentiation signaling response.

DISCUSSION

This study provides insights into the mechanisms controlling TGF-β1-dependent differentiation of fibroblasts to myofibroblasts, through the interaction of CD44 with EGFR in lipid rafts. The HA receptor CD44 can function as a co-receptor, physically associating with several membrane-bound proteins, resulting in modulation of intracellular signal transduction pathways and facilitating the formation of specialized signaling complexes (46, 47). In light of these reports, we sought to determine if a similar system operated during myofibroblast differentiation. The data reported here support our previous reports, where, following TGF-β1 stimulated differentiation, CD44 and EGFR co-localized in dermal fibroblasts (32) and also in oral fibroblasts but only if in a HA-rich environment (33).

The results reported here illustrate that EGFR was held static, at discrete, membrane-bound sites, whereas CD44 was free to diffuse within the plasma membrane. Following TGF-β1-induced differentiation, EGFR remained static, whereas the ability of CD44 to diffuse freely was attenuated as it became co-localized with EGFR. Further examination of the localization of EGFR revealed that in both fibroblasts and myofibroblasts, EGFR was associated and co-localized with areas of high cholesterol content, otherwise known as cholesterol-rich microdomains or lipid rafts (48). These findings supported previous reports of EGFR being bound in lipid raft domains in

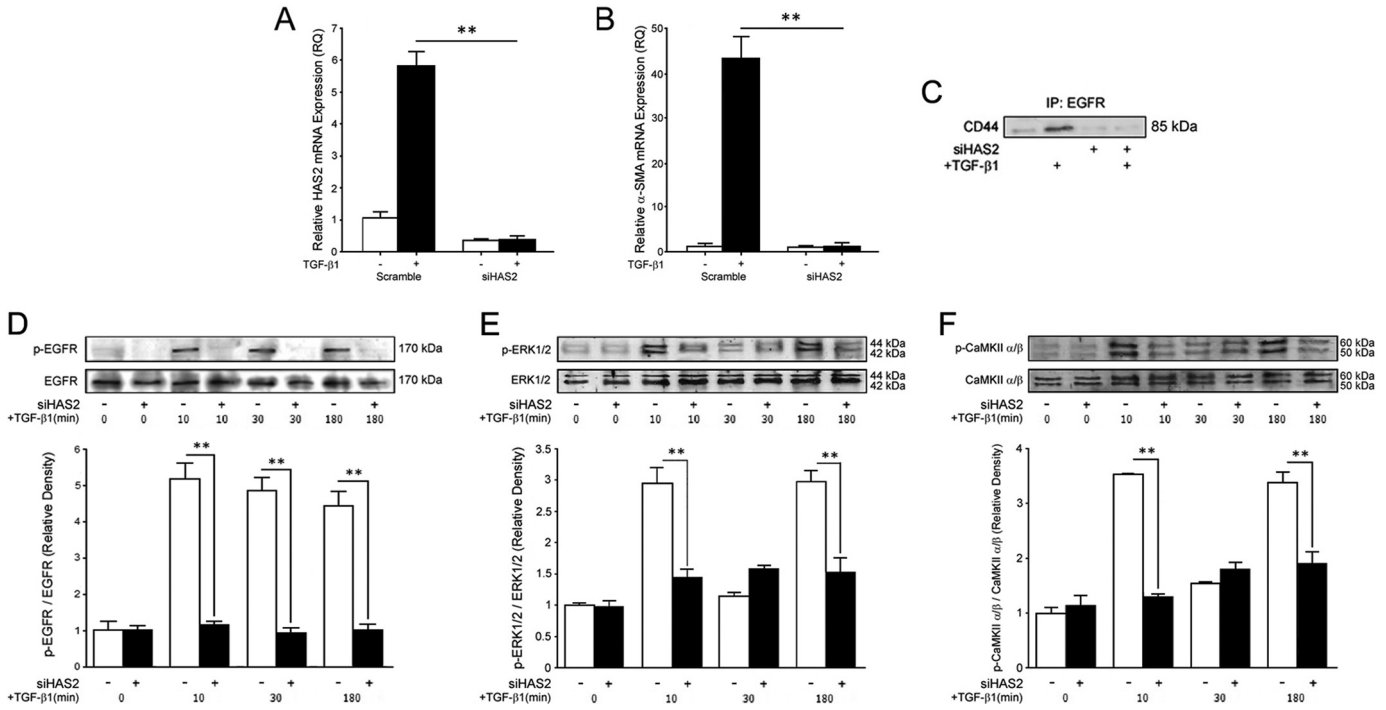

FIGURE 9. **HAS2-produced HA is required for CD44 and EGFR co-localization and subsequent signaling.** Fibroblasts were grown to 70% confluence and were growth-arrested in serum-free medium for 24 h. Subsequently, cells were transfected with scrambled siRNA (control) or HAS2 siRNA for 24 h before incubation with 10 ng/ml TGF-β1 for up to 72 h. *A*, QPCR analysis to confirm knockdown of HAS2 mRNA. Data shown are mean ± S.E. (*error bars*) of three individual experiments. *B*, QPCR was used to examine α-SMA mRNA expression. Data shown are mean ± S.E. of three individual experiments. *C*, immunoprecipitation (*IP*) of EGFR followed by immunoblotting of CD44. The image shown is representative of three separate experiments. *D*, Western blot analysis of phosphorylated (*p-EGFR*) and total EGFR at the indicated times and corrected densitometry graph. *E*, Western blot analysis of phosphorylated (*p-ERK1/2*) and total ERK1/2 at the indicated times and corrected densitometry graph. *F*, Western blot analysis of phosphorylated (*p-CaMKII*) and total CaMKII at the indicated times and corrected densitometry graph. All blots shown are representative of three separate experiments, and all densitometry graphs show mean ± S.E. of three separate experiments. **, $p < 0.01$.

other cell systems (49) and of lipid rafts as regulators of EGFR and other receptors (50, 51, 52). CD44 was found to co-localize with lipid raft domains after differentiation of fibroblasts to myofibroblasts, supporting the hypothesis that CD44 relocalization to lipid rafts containing EGFR was implicated in the differentiation pathway. Co-localization of EGFR and CD44 was lost when lipid rafts were disrupted, and these data indicate fibroblast lipid rafts as the areas where EGFR aggregated and to which CD44 moved, associating with EGFR during phenotypic change. The disruption of lipid rafts also resulted in prevention of α-SMA up-regulation following TGF-β1-induced differentiation of fibroblasts at both mRNA and protein levels, antagonizing the induction of myofibroblasts. The data reported here suggest that lipid rafts are essential structures for accommodation of EGFR-CD44 complexes and the subsequent differentiation signaling. Because CD44 motility was reduced but not completely abolished in myofibroblasts and was also found in membrane fractions positive for EEA-1, it can be concluded that CD44 is present in multiple regions of fibroblasts and myofibroblasts and indeed the cellular membrane. This coincides with previously published data that show CD44 as being bound to the cell cytoskeleton (44) and able to move to membrane-bound lipid rafts (53) and co-localize with other proteins (40, 44, 46), contributing to its repertoire of roles and cellular functions.

It is well known that TGF-β1 can induce activation of the MAPK/ERK signaling pathway. Several studies have proposed a contributory role of MAPK/ERK signaling in the promotion of the fibrotic response (54, 55) and have also shown that ERK1/2 activation is required for TGF-β1-driven proliferation in both oral and dermal fibroblasts (33). The results shown here confirm that there is a two-peak or "biphasic" activation profile of ERK1/2, dubbed the early and late signaling responses. In addition, the present study also showed a coincident biphasic activation of the kinase CaMKII at the same time points as ERK1/2, suggesting that both may be involved and play a large role in TGF-β1-dependent responses. Previous research in cancer cell lines has demonstrated that CaMKII is centrally involved in cytoskeletal reorganization and modification (44) and that HA-CD44 interaction mediated CaMKII-dependent cellular migration independently of ERK1/2 phosphorylation. In the present study, inhibition of ERK phosphorylation prevented activation of CaMKII, suggesting that ERK and CaMKII are closely associated. In contrast, inhibition of CaMKII did not attenuate ERK signaling. These data demonstrate that ERK activation is upstream of CaMKII in differentiating fibroblasts and that ERK1/2 activation is a regulator of CaMKII activation, with both required for the subsequent differentiation response.

We propose that the early ERK1/2 and CaMKII responses are involved in the induction of fibroblast differentiation, because abolition of membrane-bound lipid rafts with nystatin resulted in the attenuation of both ERK1/2 and CaMKII early waves of activation. In contrast, the late activation remained in cells pretreated with nystatin, suggesting that the late signaling

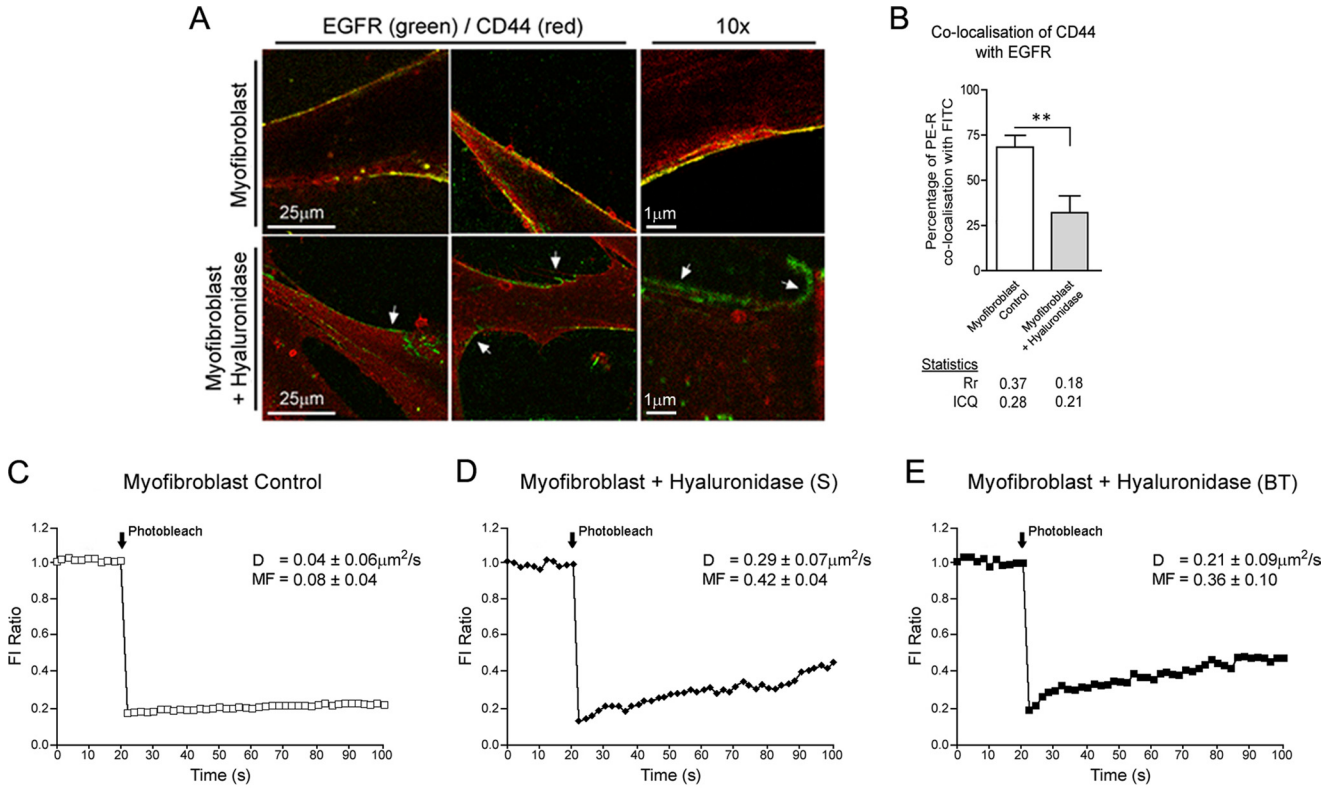

FIGURE 10. **The HA pericellular coat is required for sequestration of CD44 to EGFR and maintenance of co-localization.** *A*, myofibroblasts were grown to 70% confluent monolayers and were growth-arrested in serum-free medium for 48 h. Confocal microscopy was used to assess the effect of hyaluronidase treatments on EGFR (*green*) and CD44 (*red*) co-localization in myofibroblasts. The *white arrows* indicate areas of no co-localization. Images are representative of three individual experiments. Original magnification was ×630. *B*, graphical representation of the percentage of co-localization of PE-R (CD44) with FITC (EGFR) (Mander's co-localization coefficient). Statistical analysis includes the average Pearson's correlation coefficient (*Rr*) and ICQ for each experimental condition. Results shown are mean ± S.E. (*error bars*) of three individual experiments. FRAP was performed at 37 °C by photobleaching an ~10-μm area of the cell membrane. The recovery of fluorescence into this area was quantified and expressed as a fraction of the fluorescence intensity (*FI*) of a second region of membrane outside of the photobleached area (*FI Ratio*). Complete quantified time courses, average diffusion constants (*D*), and mobile fractions (*MF*) are shown for CD44 in myofibroblasts (*C*), CD44 in myofibroblasts treated with 1 unit of *Streptomyces* (*S*) hyaluronidase (*D*), and CD44 in myofibroblasts treated with 100 μg/ml bovine testicular (*BT*) hyaluronidase (*E*). Results are shown are representative of three independent experiments. **, $p < 0.01$.

response of ERK1/2 and CaMKII leading to proliferation was indicative of another originating source that was not in lipid raft domains. This has been suggested in research highlighting how EGFR can be susceptible to ligand-free activation and can produce a proliferation response when it has been released to non-lipid raft areas of the cell membrane (56, 57). However, it is not known whether this occurs in fibroblasts, in the absence of HA or CD44.

Several previous studies have underlined the importance of HA in fibroblast function and wound healing (22, 23, 58–60). We sought to determine whether HA synthesis and up-regulation through HAS2 were necessary steps leading to EGFR phosphorylation, receptor co-localization, and both ERK and CaMKII intracellular signaling. We investigated whether HAS2 activity was the primary modulator of the differentiation pathway, independent of the TGF-β1-SMAD signaling pathway. Here we showed that inhibition of HAS2 attenuated activation of EGFR and both signaling phases of ERK and CaMKII phosphorylation, confirming that HAS2 was an essential component in the TGF-β1-mediated differentiation pathway. We also demonstrate that removal of the HA-pericellular coat with hyaluronidase was able to release CD44 from static membrane domains, thus partially restoring its potential to move throughout the cell membrane, indicating that there may be further changes to CD44 that have taken place to maintain its association with lipid rafts and EGFR. The data presented here highlight the importance of the HA-pericellular coat in orchestrating CD44 to enable modulation of intracellular signaling pathways. Previously, we have reported that HAS2 and EGFR overexpression can restore the differentiation potential of aged fibroblasts (32). However, we have also demonstrated that HAS2 overexpression alone is not enough to initiate EGFR-CD44 coupling or differentiation and that TGF-β1 stimulation is also required (33). Our data indicate that HAS2 activation mediates differentiation through initiating CD44 sequestration into lipid rafts and the co-localization with EGFR, leading to phosphorylation of EGFR and, subsequently, ERK and CaMKII signaling. Therefore, HAS2-regulated HA synthesis is a major determining factor in the phenotypic activation of fibroblasts. This change in phenotype, however, also involves the simultaneous activation of the classical SMAD-mediated signaling pathway initiated by TGF-β1 binding to its receptor (32).

Our study provides mechanistic insights into the process of transition between scarring and scar-free tissue repair. The data presented here extend the findings from our previous research that demonstrates the important regulatory role of an HA-rich pericellular matrix in the coordination of TGF-β1-dependent fibroblast differentiation (15). Using our previous

reports together with our current findings, we propose that stimulation of differentiation in response to TGF-β1 requires an HA-rich matrix, functionality of CD44, and EGFR associated with cholesterol-rich membrane-bound lipid rafts. HA facilitates TGF-β1-dependent fibroblast differentiation through HA-CD44 binding and relocation, promoting interaction between the CD44 and EGFR within lipid rafts. This then promotes specific intracellular signal transduction through the MAPK/ERK pathway and subsequently through CaMKII, both acting to complement the SMAD pathway, resulting in fibroblast to myofibroblast differentiation.

Acknowledgments—We thank Dr. Donald Fraser and Dr. Soma Meran for helpful advice and discussion and Dr. Robert Jenkins and Dr. John Martin for technical advice.

REFERENCES

1. Grinnell, F. (1994) Fibroblasts, myofibroblasts, and wound contraction. *J. Cell Biol.* **124,** 401–404
2. Gabbiani, G. (2003) The myofibroblast in wound healing and fibrocontractive diseases. *J. Pathol.* **200,** 500–503
3. Krieg, T., and Heckmann, M. (1989) Regulatory mechanisms of fibroblast activity. *Recenti Prog. Med.* **80,** 594–598
4. Tomasek, J. J., Gabbiani, G., Hinz, B., Chaponnier, C., and Brown, R. A. (2002) Myofibroblasts and mechano-regulation of connective tissue remodelling. *Nat. Rev. Mol. Cell Biol.* **3,** 349–363
5. Border, W. A., and Noble, N. A. (1994) Transforming growth factor β in tissue fibrosis. *N. Engl. J. Med.* **331,** 1286–1292
6. Border, W. A., and Noble, N. A. (1995) Fibrosis linked to TGF-β in yet another disease. *J. Clin. Invest.* **96,** 655–656
7. al-Khateeb, T., Stephens, P., Shepherd, J. P., and Thomas, D. W. (1997) An investigation of preferential fibroblast wound repopulation using a novel *in vitro* wound model. *J. Periodontol.* **68,** 1063–1069
8. Border, W. A., and Noble, N. A. (1997) TGF-β in kidney fibrosis. A target for gene therapy. *Kidney Int.* **51,** 1388–1396
9. Hinz, B., and Gabbiani, G. (2003) Cell-matrix and cell-cell contacts of myofibroblasts. Role in connective tissue remodeling. *Thromb. Haemost.* **90,** 993–1002
10. Desmoulière, A., Geinoz, A., Gabbiani, F., and Gabbiani, G. (1993) Transforming growth factor-β 1 induces α-smooth muscle actin expression in granulation tissue myofibroblasts and in quiescent and growing cultured fibroblasts. *J. Cell Biol.* **122,** 103–111
11. Eddy, A. A. (2005) Progression in chronic kidney disease. *Adv. Chronic Kidney Dis.* **12,** 353–365
12. Desmoulière, A., Darby, I. A., and Gabbiani, G. (2003) Normal and pathologic soft tissue remodeling. Role of the myofibroblast, with special emphasis on liver and kidney fibrosis. *Lab. Invest.* **83,** 1689–1707
13. Evans, R. A., Tian, Y. C., Steadman, R., and Phillips, A. O. (2003) TGF-β1-mediated fibroblast-myofibroblast terminal differentiation. The role of Smad proteins. *Exp. Cell Res.* **282,** 90–100
14. Ito, T., Williams, J. D., Fraser, D. J., and Phillips, A. O. (2004) Hyaluronan regulates transforming growth factor-β1 receptor compartmentalization. *J. Biol. Chem.* **279,** 25326–25332
15. Meran, S., Thomas, D. W., Stephens, P., Enoch, S., Martin, J., Steadman, R., and Phillips, A. O. (2008) Hyaluronan facilitates transforming growth factor-β1-mediated fibroblast proliferation. *J. Biol. Chem.* **283,** 6530–6545
16. Kosaki, R., Watanabe, K., and Yamaguchi, Y. (1999) Overproduction of hyaluronan by expression of the hyaluronan synthase Has2 enhances anchorage-independent growth and tumorigenicity. *Cancer Res.* **59,** 1141–1145
17. Legg, J. W., Lewis, C. A., Parsons, M., Ng, T., and Isacke, C. M. (2002) A novel PKC-regulated mechanism controls CD44 ezrin association and directional cell motility. *Nat. Cell Biol.* **4,** 399–407
18. Itano, N., Atsumi, F., Sawai, T., Yamada, Y., Miyaishi, O., Senga, T., Hamaguchi, M., and Kimata, K. (2002) Abnormal accumulation of hyaluronan matrix diminishes contact inhibition of cell growth and promotes cell migration. *Proc. Natl. Acad. Sci. U.S.A.* **99,** 3609–3614
19. Ito, T., Williams, J. D., Al-Assaf, S., Phillips, G. O., and Phillips, A. O. (2004) Hyaluronan and proximal tubular cell migration. *Kidney Int.* **65,** 823–833
20. Brecht, M., Mayer, U., Schlosser, E., and Prehm, P. (1986) Increased hyaluronate synthesis is required for fibroblast detachment and mitosis. *Biochem. J.* **239,** 445–450
21. Evanko, S. P., Angello, J. C., and Wight, T. N. (1999) Formation of hyaluronan- and versican-rich pericellular matrix is required for proliferation and migration of vascular smooth muscle cells. *Arterioscler. Thromb. Vasc. Biol.* **19,** 1004–1013
22. Meran, S., Thomas, D., Stephens, P., Martin, J., Bowen, T., Phillips, A., and Steadman, R. (2007) Involvement of hyaluronan in regulation of fibroblast phenotype. *J. Biol. Chem.* **282,** 25687–25697
23. Simpson, R. M., Meran, S., Thomas, D., Stephens, P., Bowen, T., Steadman, R., and Phillips, A. (2009) Age-related changes in pericellular hyaluronan organization leads to impaired dermal fibroblast to myofibroblast differentiation. *Am. J. Pathol.* **175,** 1915–1928
24. Spicer, A. P., and McDonald, J. A. (1998) Characterization and molecular evolution of a vertebrate hyaluronan synthase gene family. *J. Biol. Chem.* **273,** 1923–1932
25. Spicer, A. P., and Nguyen, T. K. (1999) Mammalian hyaluronan synthases. Investigation of functional relationships *in vivo*. *Biochem. Soc. Trans.* **27,** 109–115
26. Jenkins, R. H., Thomas, G. J., Williams, J. D., and Steadman, R. (2004) Myofibroblastic differentiation leads to hyaluronan accumulation through reduced hyaluronan turnover. *J. Biol. Chem.* **279,** 41453–41460
27. Webber, J., Meran, S., Steadman, R., and Phillips, A. (2009) Hyaluronan orchestrates transforming growth factor-β1-dependent maintenance of myofibroblast phenotype. *J. Biol. Chem.* **284,** 9083–9092
28. Ellis, I. R., Schor, A. M., and Schor, S. L. (2007) EGF and TGF-α motogenic activities are mediated by the EGF receptor via distinct matrix-dependent mechanisms. *Exp. Cell Res.* **313,** 732–741
29. Samarakoon, R., Higgins, S. P., Higgins, C. E., and Higgins, P. J. (2008) TGF-β1-induced plasminogen activator inhibitor-1 expression in vascular smooth muscle cells requires pp60(c-src)/EGFR(Y845) and Rho/ROCK signaling. *J. Mol. Cell Cardiol.* **44,** 527–538
30. Docherty, N. G., O'Sullivan, O. E., Healy, D. A., Murphy, M., O'neill A, J., Fitzpatrick, J. M., and Watson, R. W. (2006) TGF-β1-induced EMT can occur independently of its proapoptotic effects and is aided by EGF receptor activation. *Am. J. Physiol. Renal Physiol.* **290,** F1202–F1212
31. Hardie, W. D., Davidson, C., Ikegami, M., Leikauf, G. D., Le Cras, T. D., Prestridge, A., Whitsett, J. A., and Korfhagen, T. R. (2008) EGF receptor tyrosine kinase inhibitors diminish transforming growth factor-α-induced pulmonary fibrosis. *Am. J. Physiol. Lung Cell Mol. Physiol.* **294,** L1217–L1225
32. Simpson, R. M., Wells, A., Thomas, D., Stephens, P., Steadman, R., and Phillips, A. (2010) Aging fibroblasts resist phenotypic maturation because of impaired hyaluronan-dependent CD44/epidermal growth factor receptor signaling. *Am. J. Pathol.* **176,** 1215–1228
33. Meran, S., Luo, D. D., Simpson, R., Martin, J., Wells, A., Steadman, R., and Phillips, A. O. (2011) Hyaluronan facilitates transforming growth factor-β1-dependent proliferation via CD44 and epidermal growth factor receptor interaction. *J. Biol. Chem.* **286,** 17618–17630
34. Stephens, P., Davies, K. J., Occleston, N., Pleass, R. D., Kon, C., Daniels, J., Khaw, P. T., and Thomas, D. W. (2001) Skin and oral fibroblasts exhibit phenotypic differences in extracellular matrix reorganization and matrix metalloproteinase activity. *Br J. Dermatol.* **144,** 229–237
35. Anscher, M. S., Peters, W. P., Reisenbichler, H., Petros, W. P., and Jirtle, R. L. (1993) Transforming growth factor β as a predictor of liver and lung fibrosis after autologous bone marrow transplantation for advanced breast cancer. *N. Engl. J. Med.* **328,** 1592–1598
36. Li, Q., Lau, A., Morris, T. J., Guo, L., Fordyce, C. B., and Stanley, E. F. (2004) A syntaxin 1, $G\alpha_o$, and N-type calcium channel complex at a presynaptic nerve terminal. Analysis by quantitative immunocolocalization. *J. Neurosci.* **24,** 4070–4081

37. Axelrod, D., Koppel, D. E., Schlessinger, J., Elson, E., and Webb, W. W. (1976) Mobility measurement by analysis of fluorescence photobleaching recovery kinetics. *Biophys. J.* **16,** 1055–1069
38. Zhuang, L., Lin, J., Lu, M. L., Solomon, K. R., and Freeman, M. R. (2002) Cholesterol-rich lipid rafts mediate Akt-regulated survival in prostate cancer cells. *Cancer Res.* **62,** 2227–2231
39. Tsui-Pierchala, B. A., Encinas, M., Milbrandt, J., and Johnson, E. M., Jr. (2002) Lipid rafts in neuronal signaling and function. *Trends Neurosci.* **25,** 412–417
40. Bourguignon, L. Y., Gilad, E., and Peyrollier, K. (2007) Heregulin-mediated ErbB2-ERK signaling activates hyaluronan synthases leading to CD44-dependent ovarian tumor cell growth and migration. *J. Biol. Chem.* **282,** 19426–19441
41. Zhai, H., Nakade, K., Oda, M., Mitsumoto, Y., Akagi, M., Sakurai, J., and Fukuyama, Y. (2005) Honokiol-induced neurite outgrowth promotion depends on activation of extracellular signal-regulated kinases (ERK1/2). *Eur. J. Pharmacol.* **516,** 112–117
42. Singer, H. A. (2012) Ca^{2+}/calmodulin-dependent protein kinase II function in vascular remodeling. *J. Physiol.* **590,** 1349–1356
43. Akhmetshina, A., Dees, C., Pileckyte, M., Szucs, G., Spriewald, B. M., Zwerina, J., Distler, O., Schett, G., and Distler, J. H. (2008) Rho-associated kinases are crucial for myofibroblast differentiation and production of extracellular matrix in scleroderma fibroblasts. *Arthritis Rheum.* **58,** 2553–2564
44. Bourguignon, L. Y., Gilad, E., Brightman, A., Diedrich, F., and Singleton, P. (2006) Hyaluronan-CD44 interaction with leukemia-associated RhoGEF and epidermal growth factor receptor promotes Rho/Ras co-activation, phospholipase C epsilon-Ca^{2+} signaling, and cytoskeleton modification in head and neck squamous cell carcinoma cells. *J. Biol. Chem.* **281,** 14026–14040
45. Zayzafoon, M. (2006) Calcium/calmodulin signaling controls osteoblast growth and differentiation. *J. Cell Biochem.* **97,** 56–70
46. Palyi-Krekk, Z., Barok, M., Kovacs, T., Saya, H., Nagano, O., Szollosi, J., and Nagy, P. (2008) EGFR and ErbB2 are functionally coupled to CD44 and regulate shedding, internalization and motogenic effect of CD44. *Cancer Lett.* **263,** 231–242
47. Wang, S. J., and Bourguignon, L. Y. (2006) Hyaluronan and the interaction between CD44 and epidermal growth factor receptor in oncogenic signaling and chemotherapy resistance in head and neck cancer. *Arch Otolaryngol. Head Neck Surg.* **132,** 771–778
48. Pike, L. J., and Casey, L. (2002) Cholesterol levels modulate EGF receptor-mediated signaling by altering receptor function and trafficking. *Biochemistry* **41,** 10315–10322
49. Nylander, N., Smith, L. T., Underwood, R. A., and Piepkorn, M. (1998) Topography of amphiregulin expression in cultured human keratinocytes. Colocalization with the epidermal growth factor receptor and CD44. *In Vitro Cell Dev. Biol. Anim.* **34,** 182–188
50. Roepstorff, K., Thomsen, P., Sandvig, K., and van Deurs, B. (2002) Sequestration of epidermal growth factor receptors in non-caveolar lipid rafts inhibits ligand binding. *J. Biol. Chem.* **277,** 18954–18960
51. Liu, Y., Sun, R., Wan, W., Wang, J., Oppenheim, J. J., Chen, L., and Zhang, N. (2007) The involvement of lipid rafts in epidermal growth factor-induced chemotaxis of breast cancer cells. *Mol. Membr. Biol.* **24,** 91–101
52. Irwin, M. E., Mueller, K. L., Bohin, N., Ge, Y., and Boerner, J. L. (2011) Lipid raft localization of EGFR alters the response of cancer cells to the EGFR tyrosine kinase inhibitor gefitinib. *J. Cell Physiol.* **226,** 2316–2328
53. Thankamony, S. P., and Knudson, W. (2006) Acylation of CD44 and its association with lipid rafts are required for receptor and hyaluronan endocytosis. *J. Biol. Chem.* **281,** 34601–34609
54. Ma, F. Y., Sachchithananthan, M., Flanc, R. S., and Nikolic-Paterson, D. J. (2009) Mitogen activated protein kinases in renal fibrosis. *Front. Biosci.* (*Schol. Ed.*) **1,** 171–187
55. Deng, Z. Y., Li, J., Jin, Y., Chen, X. L., and Lü, X. W. (2009) Effect of oxymatrine on the p38 mitogen-activated protein kinases signalling pathway in rats with CCl4 induced hepatic fibrosis. *Chin. Med. J.* **122,** 1449–1454
56. Lambert, S., Vind-Kezunovic, D., Karvinen, S., and Gniadecki, R. (2006) Ligand-independent activation of the EGFR by lipid raft disruption. *J. Invest. Dermatol.* **126,** 954–962
57. Pike, L. J. (2009) The challenge of lipid rafts. *J. Lipid Res.* **50,** S323–S328
58. Knudson, C. B., and Knudson, W. (2004) Hyaluronan and CD44. Modulators of chondrocyte metabolism. *Clin. Orthop. Relat. Res.* **427,** S152–S162
59. Turley, E. A., Noble, P. W., and Bourguignon, L. Y. (2002) Signaling properties of hyaluronan receptors. *J. Biol. Chem.* **277,** 4589–4592
60. Poumay, Y., and Mitev, V. (2009) Members of the EGF receptor family in normal and pathological epidermis. *Folia Med.* (*Plovdiv*) **51,** 5–17